JOURNAL OF SPACECRAFT AND ROCKETS
Vol. 38, No. 3, May–June 2001

Aerodynamic Characteristics, Database Development, and Flight Simulation of the X-34 Vehicle

Bandu N. Pamadi* and Gregory J. Brauckmann†
NASA Langley Research Center, Hampton, Virginia 23681
and
Michael J. Ruth‡ and Henri D. Fuhrmann§
Orbital, Dulles, Virginia 20166

An overview of the aerodynamic characteristics, development of the preflight aerodynamic database, and flight simulation of the NASA/Orbital X-34 vehicle is presented. To develop the aerodynamic database, wind-tunnel tests from subsonic to hypersonic Mach numbers, including ground-effect tests at low subsonic speeds, were conducted in various facilities at the NASA Langley Research Center. Where wind-tunnel test data were not available, engineering level analysis was used to fill the gaps in the database. Using these aerodynamic data, simulations have been performed for typical design reference missions of the X-34 vehicle.

Nomenclature

b	=	wing span
C_D	=	drag coefficient, drag/qS
C_i	=	generalized aerodynamic coefficient
C_L	=	lift coefficient, lift/qS
C_l	=	rolling-moment coefficient, rolling moment/qSb
$C_{l\beta}$	=	rolling moment derivative caused by sideslip
C_m	=	pitching-moment coefficient, pitching moment/$qS\bar{c}$
C_n	=	yawing-moment coefficient, yawing moment/qSb
$C_{n\beta}$	=	yawing moment derivative caused by sideslip
C_Y	=	side-force coefficient, side force/qS
$\bar{c}$	=	mean aerodynamic chord
h	=	height of the moment reference center above the ground plane
M	=	Mach number
q	=	dynamic pressure, $\frac{1}{2}\rho V^2$
S	=	reference (wing) area
V	=	velocity of air
α	=	angle of attack, deg
β	=	angle of sideslip, deg
ΔC_D	=	incremental in drag coefficient
ΔC_i	=	incremental in generalized aerodynamic coefficient C_i
ΔC_L	=	incremental in lift coefficient
ΔC_l	=	incremental in rolling-moment coefficient
ΔC_m	=	incremental in pitching-moment coefficient
ΔC_n	=	incremental in yawing-moment coefficient
ΔC_Y	=	incremental in side-force coefficient
δ_a	=	aileron deflection angle, deg
δ_{bf}	=	body-flap deflection angle, deg
δ_e	=	elevon deflection angle, deg
δ_r	=	rudder deflection angle, deg
δ_{sb}	=	speedbrake deflection angle, deg
ρ	=	density of air

Presented as Paper 2000-0900 at the AIAA 38th Aerospace Sciences Meeting, Reno, NV, 10–13 January 2000; received 23 May 2000; revision received 11 August 2000; accepted for publication 11 October 2000.

*Aerospace Engineer, Vehicle Analysis Branch, Aerospace Systems Concepts and Analysis Competancy. Associate Fellow AIAA.

†Aerospace Engineer, Aerothermodynamics Branch, Aerodynamics and Aerothermodynamics Competancy. Senior Member AIAA.

‡Technical Manager for Guidance, Navigation and Control, 21700 Atlantic Boulevard. Member AIAA.

§Aerodynamics Lead, 21700 Atlantic Boulevard. Member AIAA.

Introduction

THE X-34 vehicle being developed by the Orbital Sciences Corporation for NASA is an integral part of the reusable launch vehicle (RLV) technology program currently being pursued by NASA with industry partnership. A schematic representation of the RLV technology demonstration path is shown in Fig. 1. The primary goal of the RLV program[1] is to develop key technologies that will significantly lower the cost of access to space. The X-34 program originally started in spring of 1995 when the team of Orbital Sciences Corporation and Rockwell International was awarded a NASA contract to build an unmanned, fully reusable, two-stage, orbital vehicle capable of delivering approximately 1500-lb payload to low-Earth orbit. However, the program was canceled in late 1995 when Orbital Sciences Corporation and Rockwell International determined that the program was not economically feasible. This program was resurrected in spring of 1996 when NASA solicited proposals on a different vehicle, also designated X-34.[2] Orbital Sciences Corporation (now Orbital) was awarded this contract in June 1996.

The current X-34 vehicle is an unmanned suborbital, technology demonstrator vehicle capable of reaching an altitude of 250,000 ft and a Mach number of 8. Some of the key technologies related to RLV that will be demonstrated by the X-34 vehicle include primary and secondary composite structures, advanced thermal protection systems (TPS), low-cost avionics, rapid turnaround times, autonomous flight including landing, and all weather airplane-like operations.

The NASA Langley Research Center (LaRC) is involved in the aerodynamic analysis, wind-tunnel testing from subsonic to hypersonic speeds, and the development of the preflight aerodynamic database of the X-34 vehicle. Orbital is responsible for the flight simulation of the X-34 vehicle. An analysis of the X-34 wind-tunnel test data up to Mach 6 was reported in Ref. 3, and the formulation and development of the aerodynamic database was discussed in Ref. 4. Since then, Mach 10 wind-tunnel tests have been performed, and the database has been updated. Orbital has performed numerous simulations for various design reference mission (DRM) trajectories that are expected to be flown during the X-34 flight-test program. The objective of this paper is to present an overview of all of these activities and discuss salient aerodynamic and flight characteristics of the X-34 vehicle.

Vehicle/Mission Description

The X-34 vehicle has a close similarity with the Space Shuttle Orbiter but is relatively smaller in size. A schematic three-view diagram of the X-34 vehicle is presented in Fig. 2. The X-34 vehicle has an overall length of about 58 ft, wing span of 28 ft, and a height of about 12 ft. The approximate gross weight of the X-34 vehicle

is 45,000 lb. The main wing of the X-34 vehicle has a leading-edge sweepback of 45 deg, a dihedral of 6 deg, and an 80-deg leading-edge strake and full-span split elevons. The elevons on the same side are always deflected together. Deflected symmetrically, elevons produce pitch control, and asymmetric deflections provide roll control. The vehicle has a body flap located at the trailing edge of the fuselage. The body flap helps to shield the engine nozzle from aerodynamic heating at hypersonic speeds and also augments pitch control. The vehicle features a centerline, all-movable vertical tail for directional stability/control. The vehicle also features reaction control system (RCS) jets located at the aft end of the fuselage for roll and yaw control when the vertical tail becomes ineffective at high altitude and high Mach number (low dynamic pressure and high angles of attack) flight conditions. The vertical tail has a split speedbrake like the Space Shuttle Orbiter for energy management during descent. The TPS on X-34 consists of a mix of ceramic tiles and blankets. Ceramic tiles are used in the stagnation regions of the nose and wing leading edges where the aerodynamic heating is quite severe. Three types of blankets are employed for the rest of the acreage of the vehicle depending on the anticipated thermal environment. Additional information on the TPS can be found in Ref. 5.

The X-34 will be powered by the "Fastrac" rocket engine, which is under development at the NASA Marshall Space Flight Center (MSFC), Huntsville, Alabama. The bipropellent [liquid oxygen (LOX) and RP (kerosene)] Fastrac engine is designed for a nominal thrust of 60,000 lb and is expected to have a thrust-vectoring capability of ±15 deg in the pitch plane. The X-34 vehicle has one composite RP tank and two aluminum LOX tanks located axially one behind the other. The RP tank is located in the front part of the fuselage and ahead of the two LOX tanks.

A typical X-34 mission profile is depicted in Fig. 3. The X-34 vehicle will be "captive" carried under the belly of the L-1011 aircraft up to an altitude of about 38,000 ft and a Mach number of 0.7 at which point it will be released. The vehicle will be unpowered, and all its control surfaces will be locked for about 1 s following the drop. Once the vehicle makes a safe separation from the L-1011 aircraft, the Fastrac engine will ignite and accelerate the vehicle toward its target altitude of 250,000 ft and target Mach number of 8. After engine burn out the vehicle will coast and glide back to Earth and execute an autonomous, airplane-type landing on a conventional runway.

Flight-Test Program

The X-34 flight-test program includes L-1011 captive carry testing, runway tow testing, unpowered approach and landing tests, and incremental powered envelope expansion flights up to the full Mach 8 capability. The captive carry tests serve to validate and provide Federal Aviation Administration certification of the L-1011 as the carrier vehicle for the X-34. These tests were conducted at the NASA Dryden Flight Research Center (DFRC) in the fall of 1999 up to the maximum captive carry flight Mach number of 0.87.

At present, the X-34 vehicle is undergoing runway tow testing at the DFRC. These tests will be used to prove the autonomous landing, steering, and braking algorithms. The unpowered X-34 vehicle is towed up to a speed of about 80 mph with a truck and released. Tracking of the runway centerline, steering, and braking effectiveness are monitored during the runway tow test. Following successful completion of the runway tow test, some additional L-1011/X-34 captive carry flights and "dry run" releases will be performed to prepare for the first approach and landing test. These approach and landing tests will be conducted at the White Sands Space Harbor in New Mexico and will validate the release, approach, landing, and rollout phases of the X-34 flight profile.

The Fastrac engine will be installed on the X-34 vehicle, and static fire testing will be conducted at the Hollomon Air Force Base, New Mexico. Then, the first powered flight test at a low Mach number will be conducted at the DFRC. Subsequently, several flights will be conducted to gradually expand the flight envelope of the X-34 vehicle. It is proposed to collect aerodynamic data in these tests and use that information to update the aerodynamic database for subsequent flights. Emphasis will be placed on envelope expansion, not operability, at this point in the program. The flight testing of the X-34 vehicle will then move to NASA Kennedy Space Center (KSC), which will serve as the proving ground for X-34 operability. The X-34 vehicle will perform high Mach-number flights off the Eastern coast from North Carolina down to the KSC. Flights will be conducted every two weeks for a three month proving period with minimal ground crew. A surge capability will also be demonstrated in which the vehicle will be turned around and flown within 24 hours, which is an important requirement of the X-34 program.

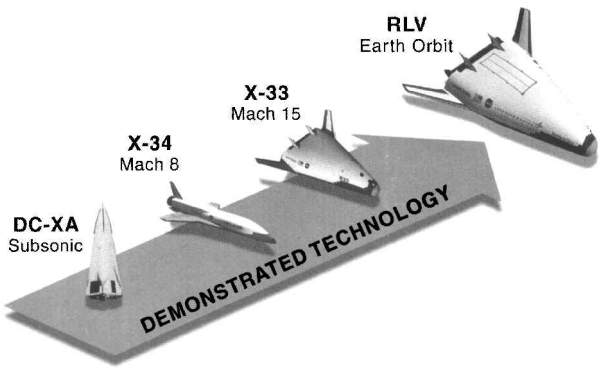

Fig. 1 RLV technology demonstration path.

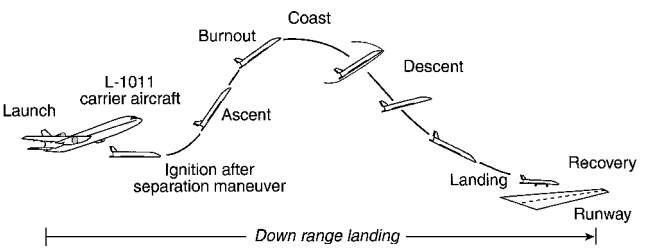

Fig. 3 Typical X-34 flight profile.

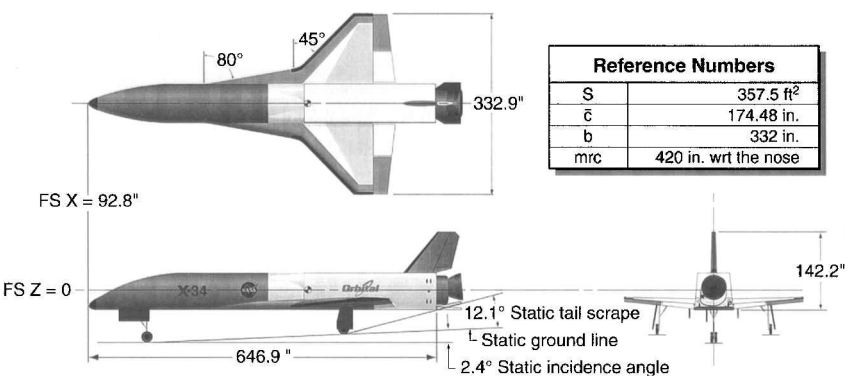

Reference Numbers	
S	357.5 ft²
c̄	174.48 in.
b	332 in.
mrc	420 in. wrt the nose

Fig. 2 Schematic diagram of the X-34 vehicle.

The X-34 program is currently planning for 27 flights. These flights include experiments to demonstrate new technologies in TPS, structures, and composite liquid oxygen tanks. Additional flight experiments may include thermal and pressure measurements for validation of computational fluid dynamics and computational aerodynamic heating codes.

Wind-Tunnel Test Facilities

A very brief description of various LaRC wind-tunnel facilities used in generating the test data included in the X-34 aerodynamic database is presented next. Detailed information on these LaRC test facilities can be found in Refs. 6–9. The L-1011/X-34 captive carry and separation aerodynamic model tests were conducted by Orbital in the Calspan transonic wind-tunnel facility. Also, some tests on the X-34 model were conducted in the Trisonic Wind Tunnel facility at MSFC. However, these test results obtained at Calspan and MSFC are not discussed in this paper because they were not used in the X-34 aerodynamic database.

LaRC 14- by 22-Foot Subsonic Tunnel

The Langley 14- by 22-Foot Subsonic Tunnel is a closed-circuit, single-return, atmospheric tunnel with a maximum speed of 338 ft/s. The test section measures 14.5×21.8 ft and has a length of about 50 ft. The maximum unit Reynolds number is 2.1×10^6 per ft. The tunnel is equipped with boundary-layer suction on the tunnel floor at the entrance to the test section.

LaRC 16-Foot Transonic Tunnel

The Langley 16-Foot Transonic Tunnel is a closed-circuit, single-return, continuous flow atmospheric tunnel. The test medium is air. This tunnel has a slotted wall, octagonal test section, which measures 15.5 ft across the flats. The normal test Mach number ranges from 0.3 to 1.3. The angle of attack can be varied up to 25 deg. The unit Reynolds number varies from 2.0×10^6 to 4.0×10^6 per ft.

LaRC Unitary Plan Wind Tunnel

The Langley Unitary Plan Wind Tunnel (UPWT) is a continuous-flow, variable-pressure, closed-circuit pressure tunnel having two separate test sections, called Low Mach Number Test Section (leg 1) and High Mach Number Test Section (leg 2). Each test section measures 4×4 ft and has a length of 7 ft. The tunnel is capable of operating from near vacuum conditions to a pressure of 10 atmospheres. The Low Mach Number Test Section covers the Mach-number range from 1.46 to 2.86 and the High Mach Number Test Section from 2.3 to 4.6. The angle-of-attack capability is from -12 to 22 deg with possibility for testing at higher values using dogleg strings. The unit Reynolds numbers range from 1.0×10^6 to 4.0×10^6 per ft.

LaRC 20-Inch Mach 6 Tunnel

The Langley 20-Inch Mach 6 Tunnel is a blowdown test facility that uses heated, dried, and filtered air as the test medium. The test section measures 20.5×20 in. Typical operating stagnation pressures range from 30 to 500 psi and the stagnation temperature from 750 to 1000°R. The unit Reynolds numbers range from 0.5×10^6 to 8×10^6 per ft. This tunnel has a capability to run continuously up to 15 min. The tunnel is equipped with a model injection system on the bottom of the test section that can insert a sheltered model into the airstream in less than 0.5 s.

LaRC 31-Inch Mach 10 Tunnel

The Langley 31-Inch Mach 10 Tunnel is a hypersonic blowdown test facility that uses dried, heated, and filtered air as the test gas. The facility typically operates at stagnation pressures ranging from 350 to 1450 psia and at a stagnation temperature of 1850°R, with corresponding freestream unit Reynolds numbers ranging from 0.5×10^6 to 2.2×10^6 per ft. A three-dimensional, contoured nozzle is used to provide a nominal freestream Mach number of 10 in the 31-Inch square test section. A side-mounted model injection system can insert models from a sheltered position to the tunnel centerline in less than 0.6 s. Run times up to 3 min are possible with this facility although current test run times were on the order of one minute.

Models, Instrumentation, and Test Procedure

The model for the 14×22 ft low subsonic freestream and ground-effect tests was a 10% scale model of the X-34 outer mold line (OML) geometry inclusive of TPS. The test model had remote activation of elevons, body flap, and rudder. The floor boundary-layer suction was used in the X-34 ground-effect tests. The ground-effect test data were obtained for various separation heights (measured from moment reference center to the ground plane) ranging from 0.3 to 2.5 times wing span. The X-34 vehicle has two doors for the main gear, one on each side, but a single door for the nose gear, only on the left side. Therefore, when the nose gear is down and its door is open, the configuration becomes aerodynamically asymmetric giving rise to side force, rolling, and yawing moments at zero sideslip. The model for the 16-Foot Transonic Tunnel and the UPWT tests was a 0.033-scale model of the X-34 OML geometry; for the 20-Inch Mach 6 Tunnel the model was a 0.018-scale model of the X-34 OML geometry; and for the 31-Inch Mach 10 Tunnel the model was a 0.013-scale model of the X-34 OML geometry.

For the test models in the 14- by 22-Foot Subsonic Tunnel, the 16-Foot Transonic Tunnel and the UPWT (leg 1) tests, boundary-layer transition trips were applied at the nose and the leading edges of the wing and vertical tail to promote turbulent flow over the test models. The boundary-layer transition trips were designed according to the procedure given in Ref. 10. However, flow diagnostic tests were not performed to verify whether the flow over the test models actually became turbulent or not as a result of tripping. The models tested in the UPWT (leg 2), the 20-Inch Mach 6 Tunnel, and the 31-Inch Mach 10 Tunnel were not tripped. However, the data from the UPWT (Leg 1) tests, where models with and without the trips were tested, showed that tripping had little effect on lift and pitching-moment coefficients but resulted in a drag coefficient increase of about 2% for Mach 1.6 to 2.5.

The aerodynamic forces and moments were measured using six component strain gauge balances. The balances used in the 20-Inch Mach 6 Tunnel and 31-Inch Mach 10 Tunnel were water cooled to minimize the balance temperature variations caused by aerodynamic heating. Corrections were applied to the balance measurements to account for the temperature effects only for the 31-Inch Mach 10 Tunnel test data. The force and moment data were acquired in a "pitch and pause" manner. The balance moment reference center (mrc), expressed in terms of full-scale vehicle, was located at 420 in. from the nose. The base and cavity pressures were measured on all models except the model in the 31-Inch Mach 10 test, and these were used to make correction to the measured axial force. In the Mach 10 tests, owing to limitations of the model and cavity size, the cavity pressure could not be measured, and no correction to the axial force was made.

In general, the tests in all of the preceding facilities covered elevon deflections from -30 to $+20$ deg, aileron deflections of -30 to $+20$ deg (elevons on one side deflected, those on the other side held at zero), body-flap deflections of -15 to $+20$ deg, rudder deflection of -5 to -30 deg, and nominal speedbrake deflections of 30 to 90 deg. For subsonic and low supersonic tests (up to Mach 2.5) the angle of attack varied from -4 to 20 deg. For UPWT (leg 2) and Mach 6 tests the angle of attack reached up to 36 deg. However, for Mach 10 tests the maximum angle of attack ranged only up to 28 deg. The sideslip was in the range of -6 to $+6$ deg for tests in the 14-by 22-Foot Subsonic Tunnel, the 16-Foot Transonic Tunnel, and the UPWT. For Mach 6 tests the sideslip was in the range -3 to $+4$ deg. In all of the tests up to Mach 6, the lateral/directional test data were obtained for angle of attack fixed with sideslip variations as well as sideslip fixed with angle-of-attack variations. However, for the Mach 10 tests, the lateral/directional test data were obtained with sideslip fixed at -3 and $+3$ deg and angle of attack varying from 0 to 28 deg.

The uncertainties in the balance force and moment coefficients for Mach numbers from 0.3 to 10 were estimated as follows: normal-force coefficient from 0.001 to 0.0216, axial-force coefficient from 0.0008 to 0.0054, pitching-moment coefficient from 0.004 to 0.0177, side-force coefficient from 0.0028 to 0.0179, rolling-moment coefficient from 0.0005 to 0.0011, and the yawing-moment

coefficient from 0.0008 to 0.004. Additional information on the measurement uncertainties can be found in Ref. 3.

Formulation of Aerodynamic Database

The development of aerodynamic models for the evaluation of the static aerodynamic forces and moments of the X-34 vehicle in free flight and for flight in ground effect is discussed in the following. This discussion does not include the control surface hinge moments and the dynamic or damping derivatives. This formulation is similar to that used in the Space Shuttle Orbiter data book.[11]

Aerodynamic Coefficients in Free Flight

Assume that the vehicle is operating in free flight (out of ground effect) at a combined angle of attack and sideslip. This assumption generally holds when the vehicle is at a height exceeding 2.5 wing spans. Let C_i represent any one of the six aerodynamic coefficients C_L, C_D, C_m, C_Y, C_l, or C_n and be given by

$$C_{i,\text{total}} = C_{i,b}(\alpha, M) + \Delta C_{i,\delta_e} + \Delta C_{i,\delta_a} + \Delta C_{i,\delta_{\text{bf}}} + \Delta C_{i,\delta_r} + \Delta C_{i,\delta_{\text{sb}}} + \Delta C_{i,\text{LG}} + \Delta C_{i,b,\beta} + \Delta C_{i,\delta_r,\beta} + \Delta C_{i,\delta_{\text{sb}},\beta} + \Delta C_{i,\text{LG},\beta} \tag{1}$$

Here the total coefficient $C_{i,\text{total}}$ is expressed as a sum of the baseline coefficent $C_{i,b}(\alpha, M)$ and various incremental coefficients ΔC_i caused by deflection of control surfaces like elevons δ_e, ailerons δ_a, body flap δ_{bf}, rudder δ_r, speedbrake δ_{sb}, or the extension of landing gear (LG), all in zero sideslip ($\beta = 0$) plus the incremental coefficients caused by sideslip for the baseline, deflection of rudder, speedbrake, and extension of the landing gear in the presence of sideslip. It is assumed that the sideslip has effect only on the baseline, and when the rudder and speedbrake are deflected, but has no effect when elevons, body flap, or ailerons are deflected. The incremental coefficient caused by a given elevon deflection δ_e is defined as

$$\Delta C_{i,\delta_e} = C_i(\alpha, M, \delta_e) - C_{i,b}(\alpha, M) \tag{2}$$

The other incremental coefficients caused by the deflection of body flap $\Delta C_{i,\delta_{\text{bf}}}$, rudder $\Delta C_{i,\delta_r}$, speedbrake $\Delta C_{i,\delta_{\text{sb}}}$, and landing gear $\Delta C_{i,\text{LG}}$ are defined in an identical manner as in Eq. (2). The parameter $\Delta C_{i,\delta_a}$ represents the incremental coefficient caused by aileron deflections and is defined in a slightly different manner. For lift, drag, and pitching-moment coefficients,

$$\Delta C_{i,\delta_a} = 0.5\left(\Delta C_{i,\delta_e=\delta_{e,L}} + \Delta C_{i,\delta_e=\delta_{e,R}}\right) - \Delta C_{i,\delta_e} \tag{3}$$

Thus, to evaluate $\Delta C_{i,\delta_a}$ the elevon aerodynamic data are used twice, once assuming $\delta_e = \delta_{e,L}$ to obtain $\Delta C_{i,\delta_e=\delta_{e,L}}$ and then assuming $\delta_e = \delta_{e,R}$ to determine $\Delta C_{i,\delta_e=\delta_{e,R}}$. As a check, when aileron deflection is zero, i.e., $\delta_{e,L} = \delta_{e,R}$, $\Delta C_{i,\delta_a} = 0$ as expected.

For the baseline in sideslip and rudder in sideslip, the incremental coefficient are defined as

$$\Delta C_{i,b,\beta} = C_i(\alpha, M, \beta) - C_i(\alpha, M) \tag{4}$$

$$\Delta C_{i,\delta_r,\beta} = [C_i(\alpha, M, \beta, \delta_r) - C_i(\alpha, M, \beta)] - \Delta C_{i,\delta_r} \tag{5}$$

The incremental coefficients caused by speedbrake deflection or the extension of the landing gear are defined in an identical manner as in Eq. (5). Additional details on the formulation of the free-flight aerodynamic database can be found in Ref. 4.

Aerodynamic Coefficients in Ground Effect

Consider the vehicle with its landing gear fully extended and operating in the proximity of the ground ($h/b \leq 2.5$). Here h is the height of the vehicle above the ground plane (assumed equal to the vertical distance between the moment reference center (mrc) and the ground plane), and b is the wing span. Let

$$C_i(\alpha, \beta, \delta_e, \delta_{\text{bf}}, \delta_{\text{sb}}, \delta_a, \delta_r, h/b) = C_i(\alpha, h/b = \infty) + \Delta C_i(\alpha, \beta, \delta_e, \delta_{\text{bf}}, \delta_{\text{sb}}, \delta_a, \delta_r, h/b) \tag{6}$$

Here it is assumed that the aerodynamic coefficient in ground effect is expressed as a sum of its value in free flight ($h/b = \infty$) for the baseline at angle of attack (zero sideslip) and an incremental coefficient caused by the deflection of the control surfaces and ground effect. The inclusion of the term h/b in the parenthesis denotes that the coefficient C_i is evaluated in ground effect. As before, C_i denotes any one of the six aerodynamic coefficients C_L, C_D, C_m, C_Y, C_l, or C_n. Assume that the incremental coefficient in Eq. (6) is given by

$$\Delta C_i(\alpha, \beta, \delta_e, \delta_{\text{bf}}, \delta_{\text{sb}}, \delta_a, \delta_r, h/b) = \Delta C_i(\alpha, h/b) + \Delta C_i(\alpha, \delta_e, h/b) + \Delta C_i(\alpha, \delta_{\text{bf}}, h/b) + \Delta C_i(\alpha, \delta_{\text{sb}}, h/b) + \Delta C_i(\alpha, \delta_a, h/b) + \Delta C_i(\alpha, \delta_r, h/b) + \Delta C_i(\alpha, \beta, h/b) + \Delta C_i(\alpha, \beta, \delta_{\text{sb}}, h/b) + \Delta C_i(\alpha, \beta, \delta_r, h/b) \tag{7}$$

Here $\Delta C_i(\alpha, h/b)$ represents the incremental coefficient for the baseline at angle of attack and in the presence of the ground with respect to the baseline in free flight ($h/b = \infty$) at the same angle of attack and is defined as

$$\Delta C_i(\alpha, h/b) = C_i(\alpha, h/b) - C_i(\alpha, h/b = \infty) \tag{8}$$

The parameter $\Delta C_i(\alpha, \delta_e, h/b)$ represents the incremental coefficient caused by elevon deflection at angle of attack and zero sideslip and in the presence of the ground with respect to the baseline in zero sideslip at the same values of α, h/b and is defined as

$$\Delta C_i(\alpha, \delta_e, h/b) = C_i(\alpha, \delta_e, h/b) - C_i(\alpha, h/b) \tag{9}$$

The incremental coefficients caused by the deflection of body flap, speedbrake, ailerons, and rudder are defined in an identical manner as given in Eq. (9). Next, consider the incremental coefficients involving sideslip. The incremental coefficients caused by sideslip are defined as

$$\Delta C_i(\alpha, \beta, h/b) = C_i(\alpha, \beta, h/b) - C_i(\alpha, h/b) \tag{10}$$

$$\Delta C_i(\alpha, \beta, \delta_r, h/b) = [C_i(\alpha, \beta, \delta_r, h/b) - C_i(\alpha, \beta, h/b)] - \Delta C_i(\alpha, \delta_r, h/b) \tag{11}$$

$$\Delta C_i(\alpha, \beta, \delta_{\text{sb}}, h/b) = [C_i(\alpha, \beta, \delta_{\text{sb}}, h/b) - C_i(\alpha, \beta, h/b)] - \Delta C_i(\alpha, \delta_{\text{sb}}, h/b) \tag{12}$$

Additional details on the formulation of ground-effect aerodynamic model can be found in Ref. 4.

Aerodynamic Database

The data in the aerodynamic database are developed in the form of tables so that the user can evaluate each of the terms appearing in the free-flight and ground-effect aerodynamic models. For the free-flight aero database the Mach number ranges from 0.3 to 10.0 with closely spaced values in the transonic regime. The angle of attack varies from -6 to 21 deg for $M = 0.3$ to 2.5 and from -5 to 40 deg for $M = 3.0$ to 10.0. The data are presented for the following cases: elevon deflections (positive downward) from -30 to 20 deg; aileron deflections from -30 to $+20$ deg (left elevons deflected, right elevons held at zero); body-flap deflections from -15 to 20 deg; rudder deflections (positive to left) from -5 to -20 deg; and speedbrake deflections (nominal) from 30 to 90 deg. The sideslip ranges from -4 to $+5$ deg. The ground-effect aerodynamic data are presented for Mach 0.3 and h/b varying from 0 to 2.5. The control deflections considered in the ground-effect aerodynamic database are similar to those in the free-flight aero database. All of the aerodynamic data in the database are with respect to the mrc located at 420 in. from the nose.

As discussed before, the lateral/directional data from the 31-Inch Mach 10 tests were obtained only for sideslip of -3 and $+3$ deg. In view of this, several gaps exist in the Mach 10 test data. To fill these gaps and populate the database at Mach 10, the Aerodynamic Preliminary Analysis System (APAS) was used. The APAS is an interactive computer code capable of providing quick engineering estimates of aerodynamic coefficients from subsonic to hypersonic

speeds.[12,13] In subsonic and low supersonic regimes APAS utilizes a combination of slender body theory, source and vortex panel distributions, and empirical methods for viscous and wave-drag estimations. For high supersonic/hypersonic speeds APAS utilizes Mark III HABP (Hypersonic Arbitrary Body Program). The HABP code uses the same geometry model as that used for subsonic/low supersonic analysis. The HABP module has various analysis options like tangent cone, tangent wedge, Newtonian impact methods, etc. The approach taken was to run APAS for Mach 6 and 10 and then calculate the incremental coefficients caused by Mach-number variation from 6 to 10 with all other parameters remaining constant. Then these incremental coefficients are added to the Mach 6 test data so as to make the Mach 6 test data applicable for Mach 10.

Results and Discussion

Aerodynamic Characteristics

Some of the salient aerodynamic characteristics of the X-34 vehicle are discussed in this section. For more details reference can be made to Refs. 3 and 4.

The variation of lift coefficient and pitching-moment coefficient with angle of attack at various Mach numbers are presented in Figs. 4 and 5. It is observed that the vehicle does not encounter stall up to 21-deg angle of attack in subsonic/supersonic range and up to 40 deg at hypersonic speeds. The vehicle is unstable at low speeds ($M = 0.3$) in pitch at low α, exhibits a pitch up tendency around $\alpha = 9$ deg, and then a stable break with further increase in α. The vehicle becomes more stable at transonic/supersonic speeds and the angle of attack at which pitch up occurs also increases as observed in Fig. 5. At hypersonic speeds the vehicle becomes unstable because of the increasing lift developed by the forward parts of the fuselage and exhibits a tendency for a stable break at high angles of attack. This type of variation in pitching-moment coefficient is typical of wing-body configurations at hypersonic speeds. The variation of untrimmed lift-to-drag ratio is presented in Fig. 6. It is observed that at low subsonic speeds the vehicle has a lift-to-drag ratio of as much as 8 at low angles of attack. However, as Mach number increases the value of lift-to-drag ratio decreases to values ranging from 1 to 2.

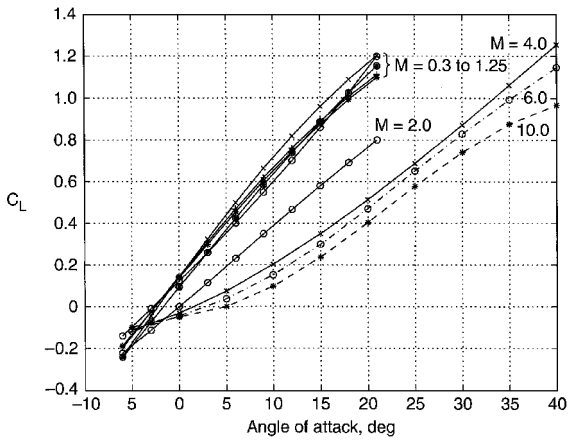

Fig. 4 Variation of lift coefficient with angle of attack for various Mach numbers.

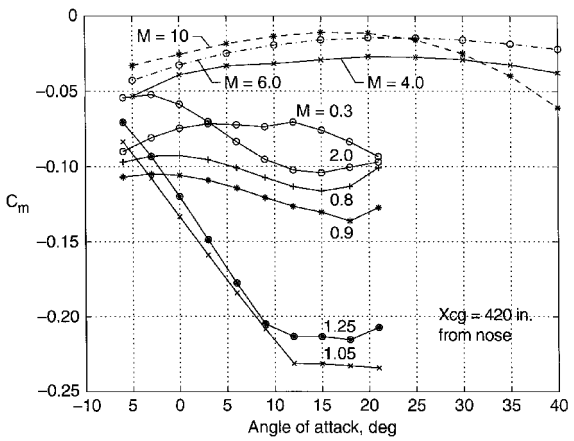

Fig. 5 Variation of pitching-moment coefficient with angle of attack for various Mach numbers.

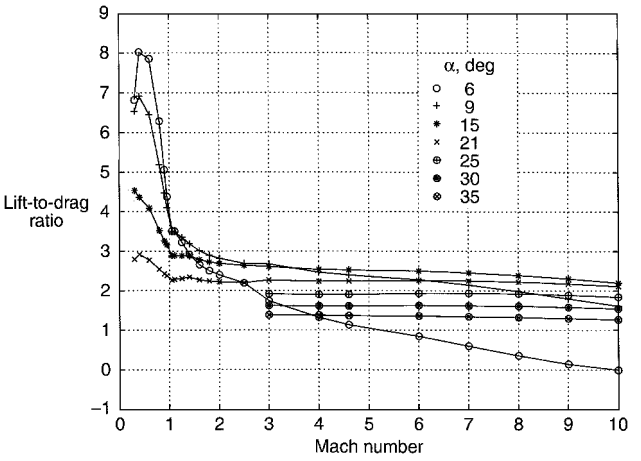

Fig. 6 Variation of lift-to-drag ratio (untrimmed) with Mach number for various angles of attack.

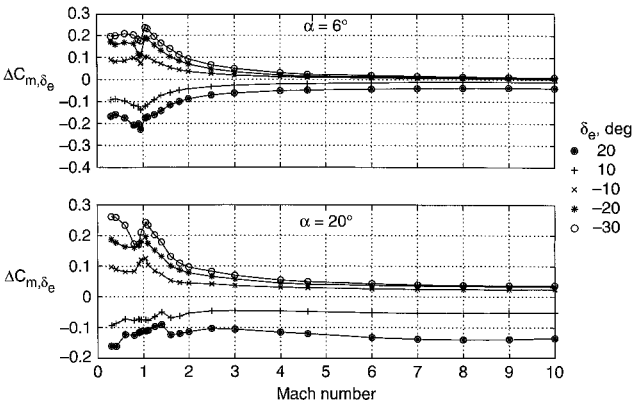

Fig. 7 Elevon effectiveness at α = 6 deg and 20 deg.

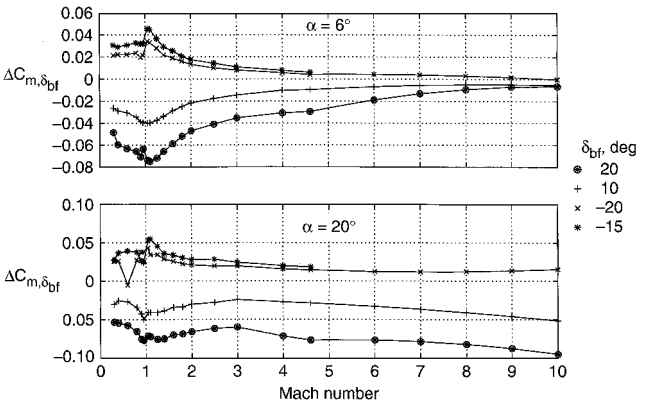

Fig. 8 Body-flap effectiveness at α = 6 deg and 20 deg.

Examples of elevon and body-flap effectiveness as measured by the incremental pitching-moment coefficient are shown in Figs. 7 and 8 for two values of angles of attack, $\alpha = 6$ and 20 deg. The aileron effectiveness as measured by the incremental rolling-moment coefficient at $\alpha = 6$ and 20 deg is presented in Fig. 9. For $\alpha = 6$ deg the effectiveness of these control surfaces decrease rapidly at supersonic and hypersonic speeds. However, for $\alpha = 20$ deg, when deflected downward, these three control surfaces retain their effectiveness all of the way up to Mach 10.

The rudder effectiveness as measured by the incremental yawing moment coefficient is shown in Fig. 10 for $\alpha = 6$ and 20 deg. It is

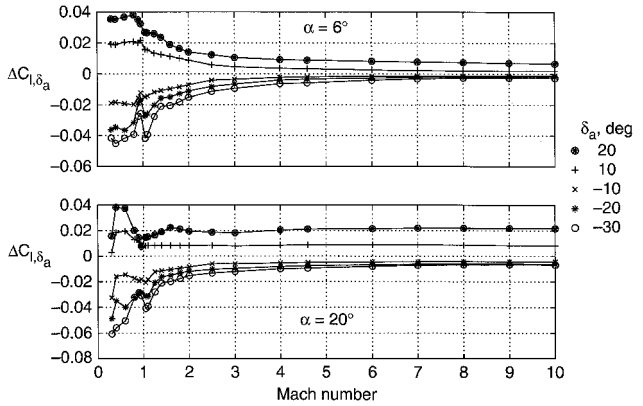

Fig. 9 Aileron effectiveness at α = 6 deg and 20 deg.

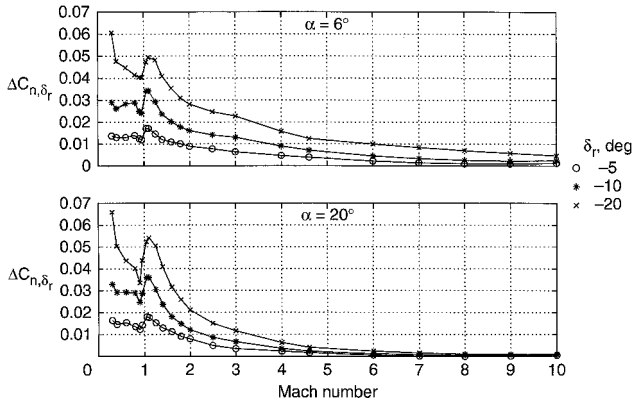

Fig. 10 Rudder effectiveness at α = 6 deg and 20 deg.

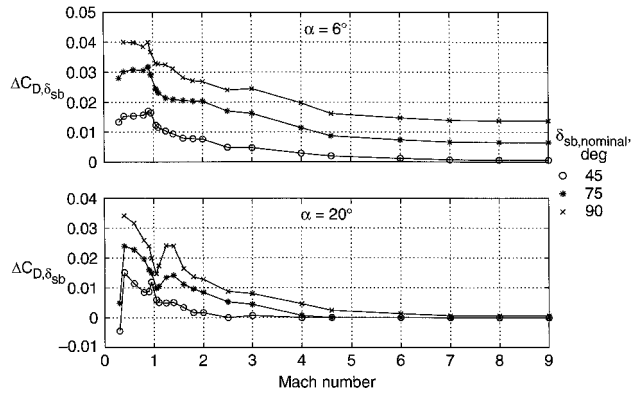

Fig. 11 Speedbrake effectiveness at α = 6 deg and 20 deg.

observed that the rudder effectiveness increases at transonic speeds but decreases rapidly at higher Mach numbers. At $\alpha = 20$ deg the rudder is virtually ineffective above Mach 5. In such situations the X-34 flight vehicle will make use of the RCS for directional control. The speedbrake effectiveness as measured by the incremental drag coefficient also varies in a similar fashion as shown in Fig. 11. The loss of rudder and speedbrake effectiveness at high angles of attack and high Mach numbers is possibly caused by the immersion of these surfaces in the low pressure wake of the fuselage and wings.

The lateral and directional stability characteristics as expressed by the parameters $C_{l\beta}$ and $C_{n\beta}$ are shown in Figs. 12 and 13. It is observed that for subsonic speeds the vehicle is stable in roll ($C_{l\beta} < 0$) at all angles of attack. Beyond Mach 1.0 it is unstable in roll ($C_{l\beta} > 0$) at low angles of attack but assumes stability at higher angles of attack. Up to Mach 1.5 the vehicle is directionally stable ($C_{n\beta} > 0$) for $\alpha \leq 12$ deg and becomes unstable for $\alpha = 18$ deg. Beyond Mach 1.5 the vehicle is directionally unstable at all angles of attack.

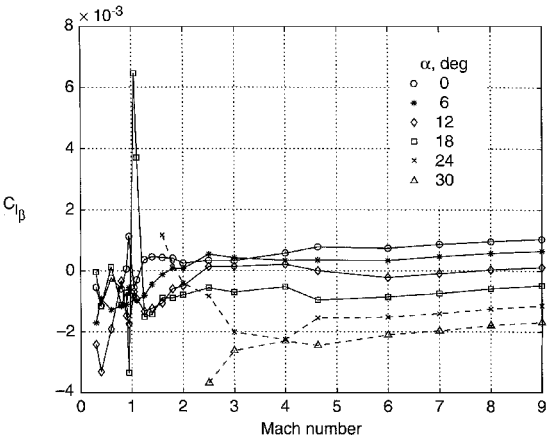

Fig. 12 Variation of lateral stability derivative $C_{l\beta}$ with Mach number for various angles of attack.

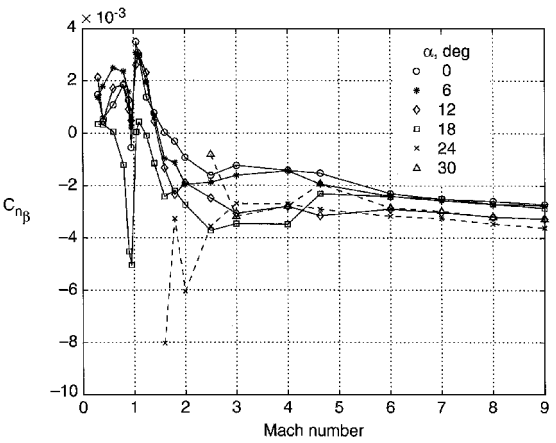

Fig. 13 Variation of directional stability derivative $C_{n\beta}$ with Mach number for various angles of attack.

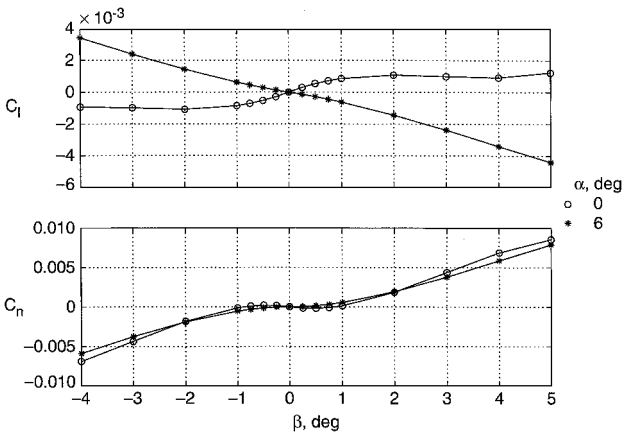

Fig. 14 Example of nonlinear variations of rolling- and yawing-moment coefficients with sideslip at M = 0.95.

In some cases the rolling and yawing moment coefficients displayed nonlinear variations with sideslip. Such nonlinear variations were particularly observed for $\alpha = 0$ to 18 deg at transonic speeds and for $\alpha \geq 12$ deg at subsonic speeds. An example of such nonlinear variation at Mach 0.95 at $\alpha = 0$ amd 6 deg is presented in Fig. 14. In view of such nonlinear behavior, the parameters $C_{l\beta}$ and $C_{n\beta}$ presented in Figs. 12 and 13 were evaluated by polynomial curve fitting the data and determining the slopes at $\beta = 0$.

The effect of landing-gear deployment at low subsonic speeds ($M = 0.3$) is shown in Figs. 15 and 16. It is observed that the landing-gear deployment leads to a more nose-down pitching moment up to 12-deg angles of attack and then the trend reverses at higher angles

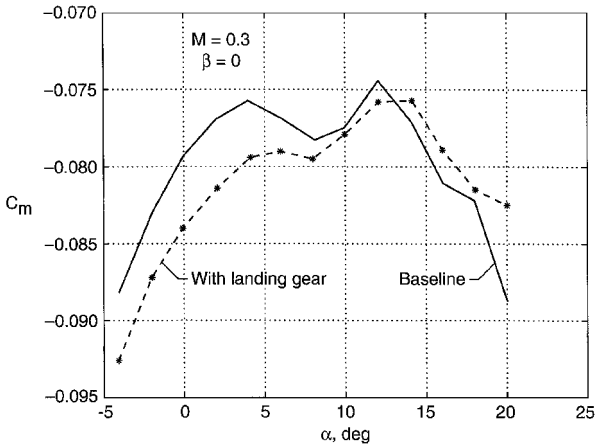

Fig. 15 Effect of landing-gear deployment on pitching-moment coefficient.

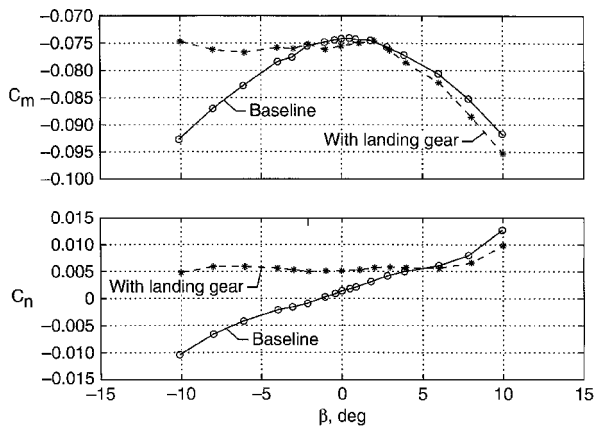

Fig. 16 Combined effect of landing gear and sideslip at $M = 0.3$, $\alpha = 12$ deg.

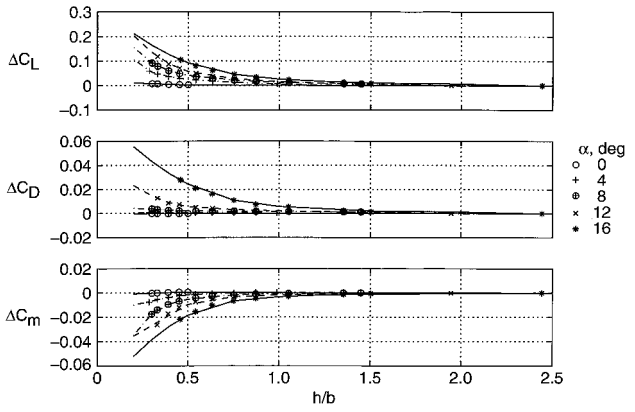

Fig. 17 Incremental lift, drag, and pitching-moment coefficients caused by baseline configuration in ground effect.

of attack. These incremental coefficients correspond to about half a degree of elevon deflection. Further, the vehicle experiences significant asymmetry in the variation of pitching-moment coefficient with sideslip and a loss of directional stability caused by landing-gear deployment as observed in Fig. 16. The asymmetry in the variation of pitching- and yawing-moment coefficients with sideslip is caused by the existence of a single nose gear door as discussed earlier.

The ground-effect aerodynamic data for the baseline configuration are shown in Fig. 17. It is observed that the incremental lift and drag coefficients are positive, whereas the pitching-moment increments are negative. This type of variation is to be expected because in the presence of the ground the strength of the wing tip vortices diminishes leading to a general reduction in downwash along the wing span and an increase in the effective angle of attack of the wing sections. In a similar fashion the elevons and body flap were

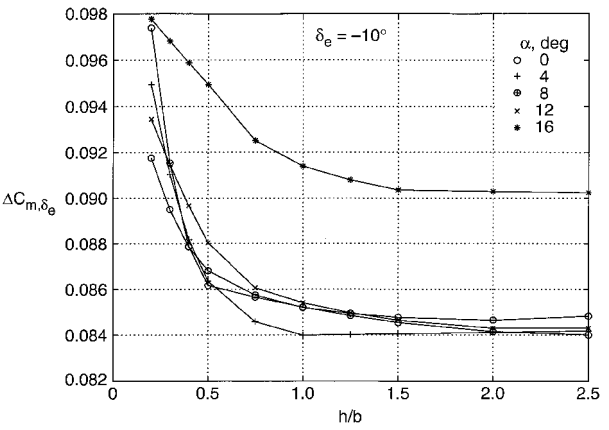

Fig. 18 Elevon effectiveness in ground effect for $\delta_e = -10$ deg.

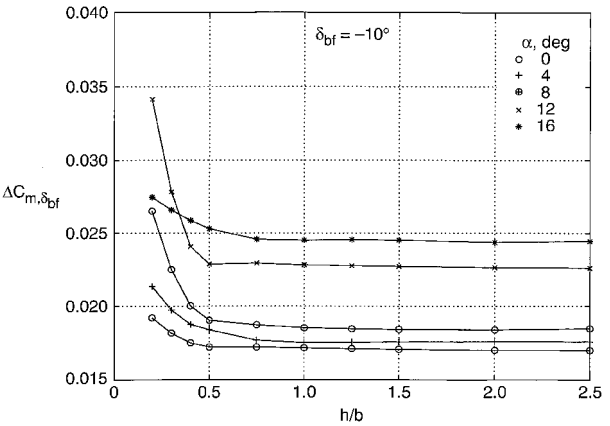

Fig. 19 Body-flap effectiveness in ground effect for $\delta_{bf} = -10$ deg.

also found to be more effective in presence of the ground compared to those in free flight as shown in Figs. 18 and 19.

The ground-effect test data were obtained for some combinations of angles of attack, sideslip, elevon, body-flap, and speedbrake deflections. These data were used to perform validation tests for the ground-effect aerodynamic model. An example of this exercise for $\alpha = 8$ deg, $\beta = 4$ deg, $\delta_e = -10$ deg, $\delta_{bf} = -10$ deg, and $\delta_{sb} = 75$ deg (nominal) is shown in Fig. 20. It is observed that the lift, drag, and pitching-moment coefficients predicted by the ground-effect aerodynamic model are within 3 or 4% of the ground-effect wind-tunnel test data for the combination of these parameters (Fig. 20a). However, the differences in the side force, rolling- and yawing-moment coefficients are much higher (Fig. 20b).

The wind-tunnel test Reynolds numbers for the X-34 model (based on mean aerodynamic chord) range up to 2×10^6, whereas corresponding full-scale flight Reynolds numbers range up to 40×10^6. The test Reynolds numbers match the flight Reynolds numbers only for a segment of the hypersonic descent. Elsewhere, the flight Reynolds numbers are orders of magnitude higher than the wind-tunnel test Reynolds numbers. To assess the impact of this on the pitch trim which is of critical importance during unpowered decent, a limited exercise was conducted using various computational fluid dynamics (CFD) codes. The results of this exercise are shown in Fig. 21. The CFD results for the tunnel Reynolds numbers are shown by open symbols, and those for the flight Reynolds numbers are shown by filled symbols. The CFD for the tunnel Reynolds numbers at Mach 1.05 and 1.25 was run with a turbulent boundary layer because the test models in the 16-Foot Transonic Tunnel were tripped. It is observed that the CFD results for Mach 2.5, 4.6, and 6.0 agree well with the wind-tunnel test data. However, the CFD for Mach 1.05 and 1.25 predicts about 10% more nose-down pitching-moment coefficient compared to the wind-tunnel test data. Further, as shown in Fig. 21, two CFD codes were run at Mach 1.05 for the flight Reynolds numbers with a turbulent boundary layer. These limited results indicate that the Reynolds number still has some

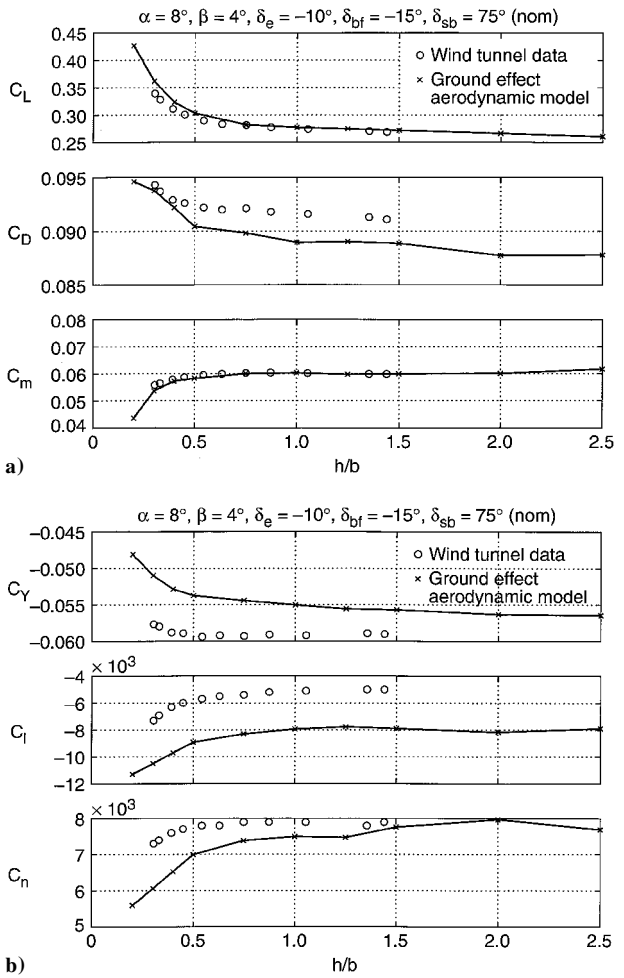

Fig. 20 Validation test for ground-effect aerodynamic model.

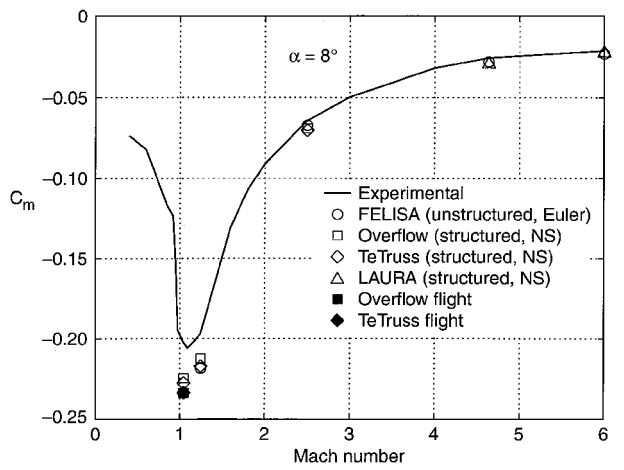

Fig. 21 Pitching-moment coefficient at wind-tunnel and flight Reynolds numbers for the baseline configuration.

influence, and, as a result, the flight vehicle is likely to experience a slightly higher nose-down pitching moment than predicted by the wind-tunnel tests and hence the data in the aero database. This increment in nose-down pitching moment approximately corresponds to about 2 deg of up elevon deflection. However, this aspect was not considered in applying the aerodynamic data in the database to the simulation of various flight trajectories presented in this paper.

Flight Simulation

Several X-34 DRM trajectories have been generated in support of the X-34 flight test program and are used for envelope expansion and flight-test range planning purposes. In this paper four of such DRM trajectories are presented. DRM 1 refers to a typical low Mach powered flight, DRM 2 refers to the maximum burn Mach 8 flight, DRM 3 refers to a no-engine ignition abort, and DRM 4 represents a nominal unpowered approach and landing flight. DRM 1, DRM 2, and DRM 3 were generated using POST,[14] and these three trajectories do not include the approach and landing phases. The DRM 4 trajectory, which includes landing-phase, was generated using STEP[15] and makes use of the ground-effect aerodynamic data in the aero database. In all of these simulations aerodynamic uncertainties including Reynolds-number effects were not considered. Further, Monte Carlo simulations incorporating aerodynamic and other uncertainties are not discussed in this paper. Such simulations are currently underway in support of the flight certification program.

The DRM 1 is representative of the first powered (low Mach number) flight of the X-34 vehicle. After separation from the L-1011, the vehicle begins a pull up to engine ignition attitude. The engine is ignited, and the vehicle continues a 2-*g* pull up maneuver. The maximum dynamic pressure attained during this flight is about 600 lb/ft.^{2} The engine burn is cut off at a point when about 50% propellants are still remaining in the tanks. At this point the vehicle dumps the remaining propellants and glides back to execute a standard approach and landing.

The variations of the trajectory parameters for DRM 1 are presented in Fig. 22, and time histories of the control surface deflections are shown in Fig. 23. The maximum altitude reached is about 115,000 ft, the maximum Mach number reached is about 3.6, and the angle of attack goes up to about 14 deg during the pull up following the drop. The thrust vectoring (gimbal angle) of about 15 deg in pitch plane is commanded initially during the ascent to augment the pitch control. The commanded elevon deflection reaches about −20 deg when the vehicle is descending around Mach 3. With the full-scale vehicle likely to experience more nose-down pitching moment that approximately needs an additional −2-deg elevon deflection to trim as discussed earlier, the actual commanded elevon deflection could be about −22 deg. Although the commanded elevon deflections are

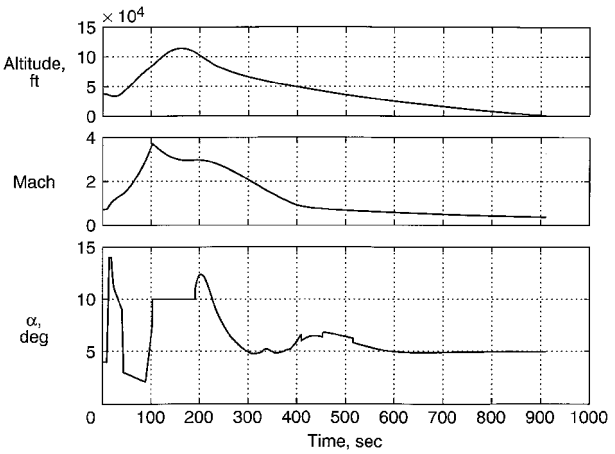

Fig. 22 Time histories of altitude, Mach number, and angle of attack for DRM 1.

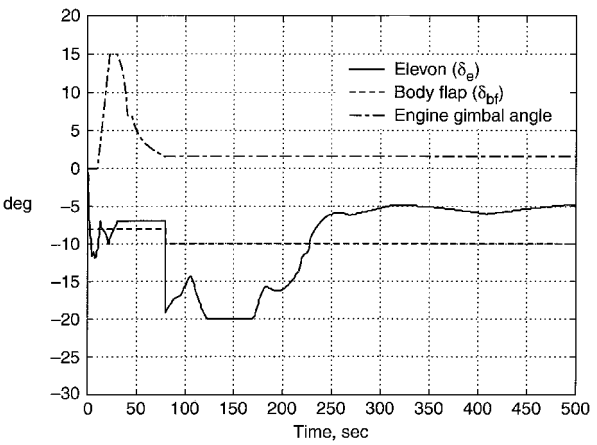

Fig. 23 Time histories of control surface deflection for DRM 1.

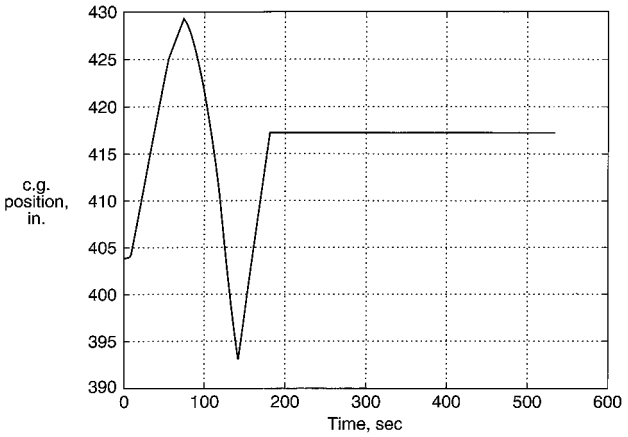

Fig. 24 Variation of c.g. during flight for DRM 1.

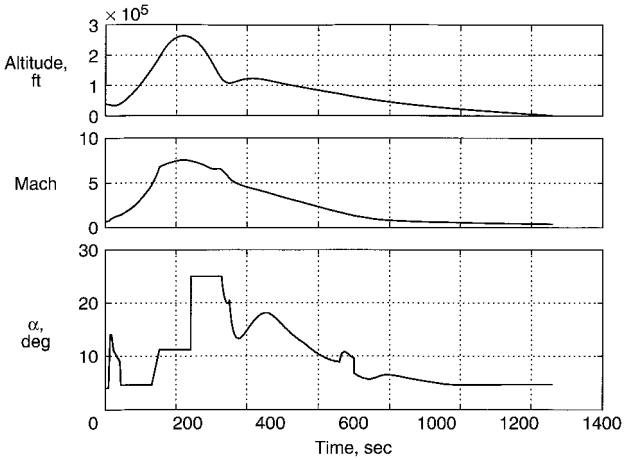

Fig. 25 Variation of altitude, Mach number, and angle of attack for DRM 2.

significantly high, these values are still within the permissible limits. The commanded body-flap deflections go up to −7.5 deg during the initial part of the ascent, and for the rest of the trajectory the body-flap deflection remains at −10 deg. The variation of c.g. position is shown in Fig. 24. At drop the c.g. is located at about 404 in from the nose of the vehicle. During the DRM1, at first the c.g. moves aft to about 430 in. and then moves forward to about 393 in and again moves aft to about 417 in. After the engine burn cutoff the c.g. remains constant at 417 in. This pattern of c.g. movement is caused by the manner in which LOX (liquid oxygen) was consumed during the flight. The LOX is consumed first from the forward tank causing the c.g. to move aft. The subsequent forward shift followed by another rearward movement and remaining constant around 417 in. is on account of sequential RP (kerosene) and LOX dump.

The DRM 2 is representative of a full-engine burn to propellant depletion and vehicle reaching the designated altitude of 250,000 ft and target speed of Mach 8. The sequence of separation, engine ignition, and pull up are similar to the DRM 1. During this flight, the vehicle spends some time outside the atmosphere (dynamic pressure less than 1 psf) and performs an entry at 25-deg angle of attack. Because the aerodynamic controls are ineffective under such circumstances, the vehicle utilizes RCS during the high-altitude flight for lateral/directional control. However, the design and analysis of the RCS system was outside the scope of this study. The vehicle then follows the standard approach and landing flight path. Stagnation temperatures during entry can reach 2000°F. Envelope expansion flights will fill the gap between the low Mach DRM 1 flight and the maximum Mach 8 DRM 2 mission. The variations of the trajectory parameters for DRM 2 are presented in Figs. 25 and 26. The vehicle attains its target altitude of 250,000 ft and target speed of Mach 8 around 220 s and then starts its unpowered descent with an angle of attack of about 25 deg. The commanded elevon deflections reach about −16 deg while the vehicle is passing through

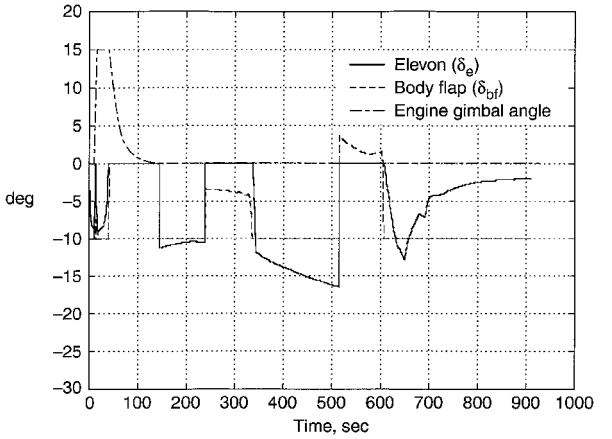

Fig. 26 Time histories of control surface deflections for DRM 2.

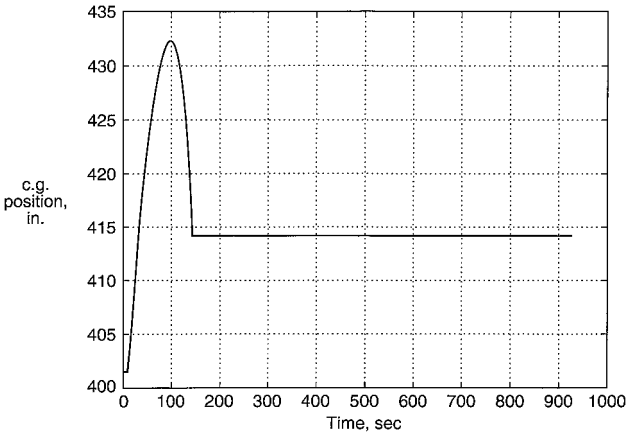

Fig. 27 Variation of c.g. during flight for DRM 2.

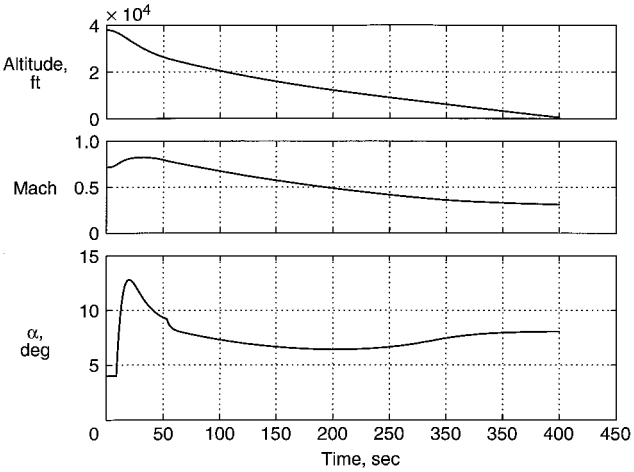

Fig. 28 Time histories of altitude, Mach number, and angle of attack for DRM 3.

supersonic/transonic speeds. The variation of the c.g. position is shown in Fig. 27. The c.g. moves aft initially because of consumption of LOX from forward tank and then it moves forward because of depletion of aft LOX tank. The c.g. then remains constant at about 414 in when all of the propellants are depleted and engine burn out occurs.

The DRM 3 is an abort trajectory to deal with engine failures. Should the main engine fail to ignite after separation, a DRM 3 abort mission would be initiated in which propellants are immediately dumped, and an approach and landing to the abort site is conducted. As the full propellant load is dumped, the c.g. can vary greatly. The DRM 3 abort mission is not a planned flight, but would only occur in the case of engine ignition failure. The variations of trajectory parameters for DRM 3 are shown in Figs. 28 and 29. The

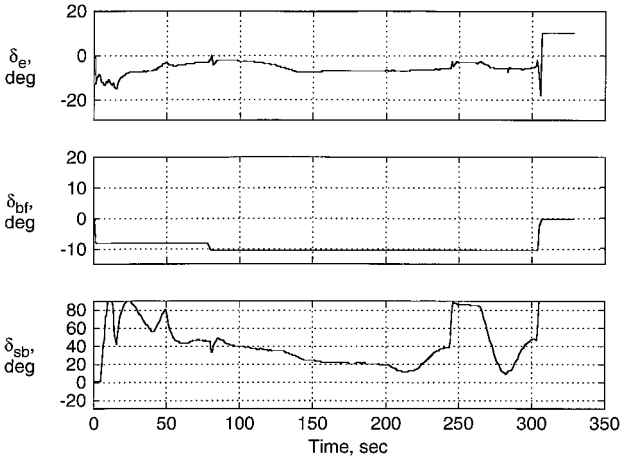

Fig. 29 Time histories of control surface deflections for DRM 3.

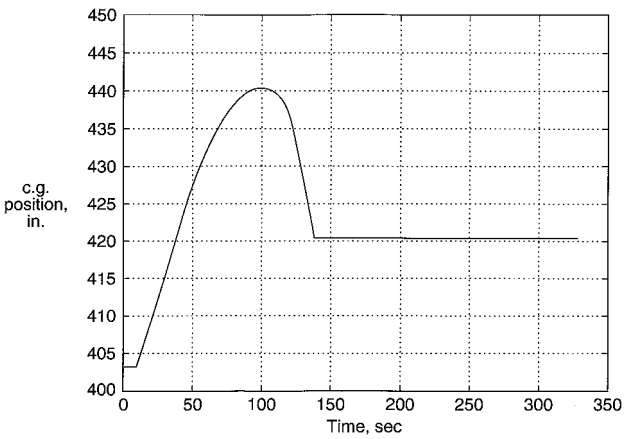

Fig. 30 Variation of c.g. during flight for DRM 3.

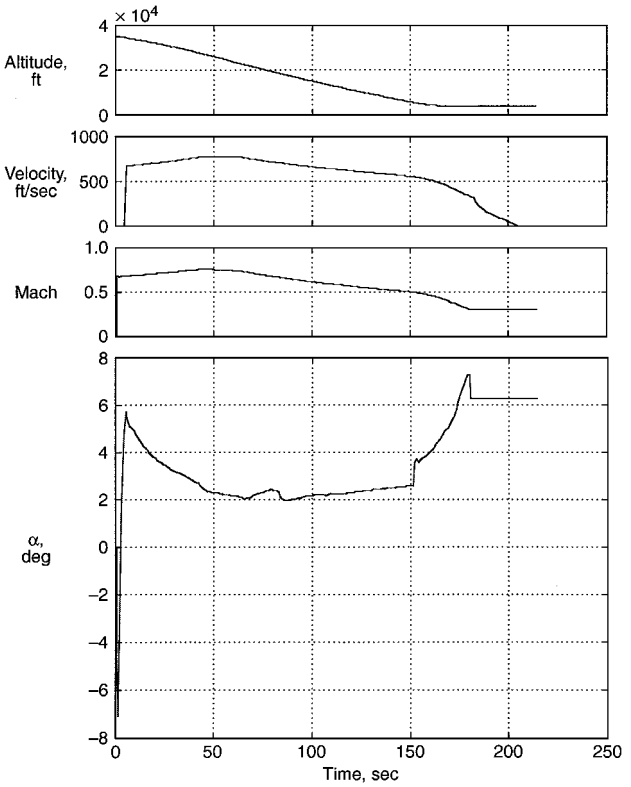

Fig. 31 Time histories of altitude, velocity, Mach number, and angle of attack for DRM 4.

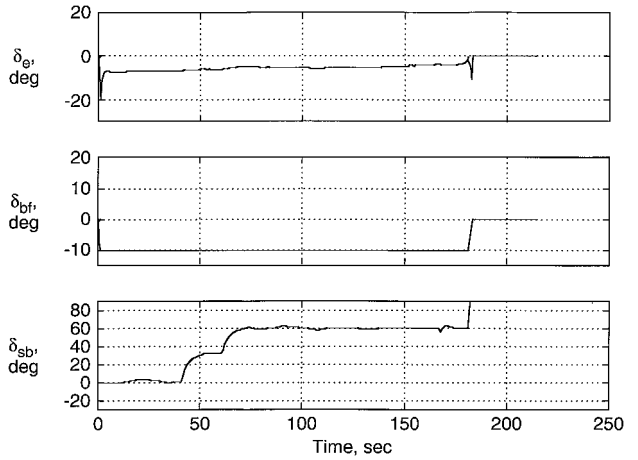

Fig. 32 Time histories of control surface deflections for DRM 4.

altitude and Mach number steadily decrease following the initiation of the abort maneuver. The commanded elevon deflections reach up to −20 deg toward the end. As discussed before for DRM 2, even though these elevon deflections are significantly high they are still within permissible limit. The commanded speedbrake deflections reach up to 80 deg at the beginning and toward the end of this mission. Note that the speedbrake deflections were not commanded during DRM 1 and DRM 2. The variation of the c.g. is shown in Fig. 30. The initial aft movement of the c.g. followed by the forward movement and then subsequently a constant position around 420 in. are all caused by the sequential dumping of the RP and LOX.

The unpowered approach and landing test (DRM 4) will constitute the first unpowered flight of the X-34 vehicle. After release from the L-1011, the unfueled X-34 acquires the approach flight path and conducts a standard approach and landing. The variations of the trajectory parameters for DRM 4 are shown in Figs. 31 and 32. It is observed that the vehicle lands with an angle of attack of approximately at 6.2 deg. The commanded elevon, body-flap, and speedbrake deflections are within limits as in DRM 1 to DRM 3.

Summary

This paper has presented an overview of the aerodynamic characteristics, the development of the preflight aerodynamic database, and flight simulations of the NASA/Orbital X-34 vehicle. The aerodynamic data in the database are provided for both free flight and for final approach and landing conditions (ground effect). The database covers the complete range of Mach numbers, angles of attack, sideslip, and control surface deflections expected in the entire flight envelope of the X-34 vehicle. The variations of the trajectory parameters and control time histories for four design reference missions, which are representative of the X-34 flight test program, indicate that the vehicle performs these missions satisfactorily, and the commanded control deflections are within the permissible limits at all points along these flight trajectories.

Acknowledgments

The authors are thankful to Jim Weilmuenster, Ken Sutton, Peter Buning, Ram Prabhu, and Shahyar Pirzadeh of NASA Langley Research Center for the CFD calculations.

References

[1]Freeman, D. C., Jr., Talay, T. A., and Austin, R. E., "Reusable Launch Vehicle Technology Program," International Astronautical Federation, Paper 96-V.4.01, Oct. 1996.

[2]NASA, "Reusable Launch Vehicle (RLV), Small Reusable Booster, X-34," Cooperative Agreement Notice, CAN 8-2, Jan. 1995.

[3]Brauchmann, G. J., "X-34 Vehicle Aerodynamic Characteristics," *Journal of Spacecraft and Rockets*, Vol. 36, No. 2, 1999, pp. 229–239.

[4]Pamadi, B. N., and Brauchmann, G. J., "Aerodynamic Characteristics and Development of the Aerodynamic Database of the X-34 Reusable Launch Vehicle," International Symposium on Atmospheric Reentry Vehicles and Systems, Association Aeronautique et Astronautique de France, Paper 17.1, Paris, March 1999.

[5]Wurster, K. E., Riley, C. J., and Zoby, E. V., "Engineering Aerothermal Analysis for X-34 Thermal Protection System Design," *Journal of Spacecraft and Rockets*, Vol. 36, No. 2, 1999, pp. 216–228.

[6]Gentry, C. E., Quinto, P. F., Gatlin, G. M., Gregory, M., and Applin, Z. T., "The Langley 14- by 22- Foot Subsonic Tunnel: Description, Flow Characteristics and Guide for Users," NASA TP-3008, Sept. 1990.

[7]Capone, F. J., Bangert, L. S., Asbury, S. C., Mills, C. T., and Bare, E. A., "The NASA Langley 16- Foot Transonic Tunnel," NASA TP-3521, Sept. 1995.

[8]Jackson, C. M., Corlett, W. A., and Monta, W. J., "Description and Calibration of the Langley Unitary Plan Wind Tunnel," NASA TP-1905, Nov. 1981.

[9]Micol, J. M., "Hypersonic Aerodynamic/Aerothermodynamic Testing Capabilities at Langley Research Center: Aerodynamic Facilities Complex," AIAA Paper 95-2107, June 1995.

[10]Braslow, A. L., "Simplified Method for Determination of Critical Height of Distributed Roughness Particles for Boundary Layer Transition at Mach Numbers from 0 to 5," NACA TN D-4363, Sept. 1958.

[11]"Aerodynamic Design Data Book, Vol. I, Orbiter Vehicle," Rockwell International Space Div., Rept. SD 72-SH-0060-1L, Downey, CA, Nov. 1977.

[12]Bonner, E., Clever, W., and Dunn, K., "Aerodynamic Preliminary Analysis System II, Part I—Theory," NASA CR-182076, April 1991.

[13]Sova, G., and Divan, P., "Aerodynamic Preliminary Analysis System II, Part II—User's Manual," NASA CR-182077, April 1991.

[14]Brauer, G. L., Cornick, D. E., and Stevenson, R., "Capabilities and Applications of the Program to Optimize Simulated Trajectories (POST)," NASA CR-2770, Feb. 1977.

[15]"STEP: PEGASUS NASA 'Six Degree of Freedom (6DOF) Simulation User's Manual," Orbital, TM-11787, Dulles, VA, 30 June 1995.

R. M. Cummings
Associate Editor